Optics Communications 284 (2011) 4577–4583

Contents lists available at ScienceDirect

Optics Communications

journal homepage: www.elsevier.com/locate/optcom

Evaluation of lab-scale EUV microscopy using a table-top laser source

Davide Bleiner [a,*], Felix Staub [a], Vitaliy Guzenko [b], Yasin Ekinci [b], Jürg E. Balmer [a]

[a] Institute for Applied Physics, University of Bern, CH 3012, Berne, Switzerland
[b] Paul Scherrer Institut (PSI), Laboratory for Micro & Nanotechnology, CH-5232 Villigen, Switzerland

ARTICLE INFO

Article history:
Received 28 January 2011
Received in revised form 6 April 2011
Accepted 18 May 2011
Available online 1 June 2011

Keywords:
Extreme Ultraviolet
X-ray laser
Nano-imaging
Siemens Star

ABSTRACT

High brightness Extreme Ultraviolet (EUV) sources for laboratory operation are needed in nano-fabrication and actinic ("at-wavelength") inspection of the masks for high volume manufacturing in next generation lithography. Laser-plasma EUV sources have the required compactness and power scalability to achieve the demanding requirements. However, the incoherent emission lacks the brightness for single-shot high contrast imaging. On the other hand, fully coherent sources are considered to be unsuitable for full-field sample illumination and prone to speckles. We evaluate the capabilities of a lab-scale amplified-spontaneous-emission (ASE) EUV laser source to combine brightness and high quality imaging with full-field imaging, along with rapid acquisition and compactness.

1. Introduction

The semiconductor industry has invested a remarkable amount of resources to prepare the transition to Extreme Ultraviolet (EUV) lithography using 13.5-nm plasma sources [1]. The main challenges have been related to the average power that lab-scale sources could attain, presently demonstrated to just a few Watts, and the uptime, limited to a few hours. If the former is an issue that seems to be addressable by using more powerful and multiplexed drivers, it is nevertheless coupled with a consistent increase of debris that can rapidly hamper the source functionality and limit the uptime. Nevertheless a 1–100 kHz repetition rate is expected to provide demo-level average power of a few tens of Watts and enable EUV lithography by 2017. The latter, however, requires also rapid mask inspection to make sure that printable defects are below a critical density, and guarantee a profitable wafer yield of 80–100 good wafer/h [1].

Mask inspection devices, operating at EUV wavelengths, are thus an important enabling tool for the overall implementation of EUV lithography. A main difference between inspection and printing tools is that the former does not need excessive average power, important for high throughput, rather should provide the brightness for high contrast imaging. Unfortunately, high magnification degrades illumination. Thus high photon flux in a narrow angle (brightness or spatial coherence) is important. Moreover, high resolution attained with short wavelength sources relaxes requirements on large NA, which otherwise introduces spherical aberration.

Brightness is the bandwidth intensity per unit solid angle, and is therefore enhanced in a conjunct effort to enhance (i) the number of in-band photons emitted (ii) within a narrow collimation angle. *Spontaneous emission* is a 4π sr irradiation, requiring collection optics. The use of collector optics determines the effective source numerical aperture (NA). Large NA collection maximizes the photon flux but deteriorates the source projection by poorer collimation. *Amplified spontaneous emission (ASE)* is, on the contrary, characterized by a pronounced directionality of light propagation. In this respect, ASE laser sources have implicitly higher brightness thanks to the primary collimated emission of the photon bunch.

Brightness is important for high contrast imaging, because directionality of light reduces image shadowing effects. Thus, bright-to-dark transitions at the feature's border can be as steep as the morphology dictates. High brightness demands high spatial coherence. The longitudinal coherence, or *monochromaticity*, is important to have sharp diffraction-limited images. The transverse coherence, or *collimation*, should not be excessive, in order to avoid occurrence of speckle interference and to enable full aperture illumination (full field).

Typically, high brightness at EUV is a characteristic of large-scale facilities, such as synchrotrons and free-electron lasers (FEL). The excessive cost-of-ownership of such large facilities has bottlenecked their access in research and prevented implementation in the industry. Therefore, the need for high brilliance lab-scale EUV sources is strategic for either boosting research or enabling industrial productivity.

Plasma sources generated by laser irradiation of a target material have been proposed to fill this gap. Laser-driven plasma sources are based on optical energy conversion from a driver IR pulse. The latter irradiates a target material and induces a hot and dense plasma

* Corresponding author. Tel.: +41 31 631 85 29
E-mail address: bleiner@iap.unibe.ch (D. Bleiner).

0030-4018/$ – see front matter © 2011 Elsevier B.V. All rights reserved.
doi:10.1016/j.optcom.2011.05.047

that radiates in the desired bandwidth. The target material largely contributes with the characteristic spectrum of the atomic ensemble. For EUV lithography application, Sn has been identified as the most efficient target material. The spontaneous emission spectrum has been investigated elsewhere [2,3], showing an unresolved transition array (UTA) around 13.5 nm from the emission of several ionization stages between Sn^{5+} and Sn^{13+}. Depending on the form of the target, i.e. whether gaseous [4], mass-limited [5], or solid [6], the occurrence of *Bremsstrahlung* as well as *debris* can vary, degrading the source cleanliness. The UTA emission is Lambertian and thus requires large collection optics (300–600 mm in diameter) to be directed to the intermediate focus. Provided that good thermo-mechanical stability is accomplished, the collection optics is aged as a consequence of the exposure to ionizing radiation as well as fast ion debris.

Alternatively, for a very hot (e.g. 510 eV) and dense (e.g. 10^{20} to 10^{21} cm^{-3}) plasma conditions induced along a line focus (plasma column), the closed-shell Ni-like Sn ion sustains amplified spontaneous emission (ASE) of the $4d^1S_o$–$4p^1P_1$ lasing transition at 11.97 nm [7]. The laser emission is inherently of high brilliance because directional and subtended within a few milliradians of solid angle. The radiation characteristics are such that small optics (1 in. or less) can be used and positioned away from the zone of debris showering.

In this paper we report on imaging capabilities of a compact footprint EUV laser facility, developed at the University of Berne, to the imaging obtained with spontaneous emission. The compactness of the EUV laser source demonstrates that high brightness imaging is now accessible on a laboratory scale.

2. Architecture of the BEAGLE table-top x-ray laser and imaging setup

The present work is performed at the BEAGLE (Bern Advanced Glass Laser for Experiments) facility at the University of Berne. A terawatt drive laser beam is used to irradiate a metallic tin target and induce a plasma, which acts as gain medium to amplify spontaneous emission (ASE). The drive beam is a 1054-nm (IR) Nd:glass laser with a pulse duration of 1.2 ps and an energy delivered onto the target, which was limited to 2.5–3 J for the tin laser. The oscillator feeds pulses of approx. 200 fs at a repetition rate around 100 MHz, having energies of a few nJ. A Pockels cell gates one pulse to the pulse stretcher and amplification stage. The pulse stretcher consists of a grating pair of 1740 grooves/mm. The pulse is, prior to amplification, stretched to 1 ns. The pre-amplification is done in a regenerative amplifier with a total of ca. 50 round-trips, 7.1 ns round-trip time, and overall gain of approx. 10^6 with output in the mJ level. This is a compact and effective way of pre-amplification. Pulse contrast is approx. 1000:1. A set of amplification Nd:glass rods, with diameters 10 mm, 16 mm, 25 mm, 45 mm contributes to the generation of a Joule-level pulse, which is finally compressed with another grating pair. Pulse compression is done with a double-pass grating compressor with one grating tilted by 0.09°, such that a traveling wave at the speed of light is attained even at an incidence angle of 45° [8]. Prepulses induced in the regenerative amplifier are suppressed by means of Pockels-cell gating on the amplifier chain. The spatial beam profile is homogenized and image-relayed by means of four evacuated spatial filters at 10^{-4} mbar to avoid the formation of hot spots. Two prepulses and a main pulse of identical duration are delivered at 45° onto the target. The spatial overlap is checked adjusting the position of a set of beamsplitters with 0.25%, 8%, and 100% reflectivity, respectively.

Spectral characteristics of the EUV laser (Fig. 1) have been determined using an on-axis, time-integrating spectrometer that provided 2D images of angle- and wavelength-dispersion. The spectrometer consists of a 1200 mm^{-1} flat field Hitachi grating (radius of curvature 5649 mm), working at grazing-incidence of 3°. The grating disperses the radiation onto a 40-mm-diameter P20 phosphor screen, imaged onto a cooled CCD camera with a pixel size

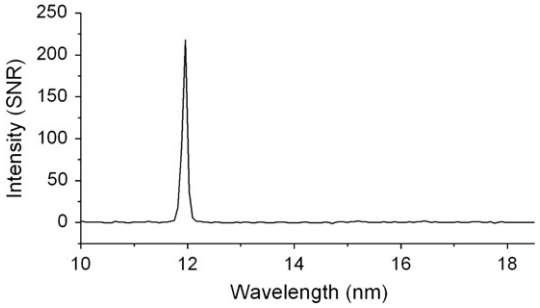

Fig.1. Spectral characteristics of the EUV laser source using a Sn target.

of 25 μm. The spectral range is between 5 and 25 nm with a resolution of approx. 0.1 nm limited by slitless operation of the spectrometer.

Planar diamond-machined tin targets (99.9% Sn) were irradiated with fresh surface at every shot. The target chamber was operated at ca. 10^{-4} mbar and connected to the diagnostics chamber at 10^{-6} mbar by means of a vacuum gate and with a cold finger to prevent condensation on the CCD detector. The EUV was detected using a 16-bit 1024×1024-pixel back-illuminated x-ray CCD with a pixel size of 13 μm. The chip was cooled to −20 °C for low background level. The optical setup for EUV microscopy was optimized using in-house developed optics software for raytracing. The imaging setup is shown in Fig. 2.

The microscope is composed of four Mo/Y multilayer mirrors (R = 48% centered at 12 nm [9]): (i) a planar mirror, (ii–iii) a condenser — objective spherical pair with focal lengths of 120 mm, (iv) a 45° planar mirror directing the rays to the CCD detector, through a 150-nm Zr foil that provides 60% transmission in the 7–14 nm and blocks radiation at longer wavelengths. The CCD detector was located at 1650 mm from the objective, which resulted in a 12× magnification. The illuminated field of view was approx. 100×50 μm and the resolution below 1 μm, limited by magnification of the available optics. The images were obtained with one single shot, since the photon flux of ca. 10^{11} photons/shot was enough for good signal-to-noise ratio.

A particular transmission imaging sample (Fig. 3) was used to evaluate the resolution of optical instruments ("Siemens star"). It consisted of a pattern of transmitting spokes on a dark background, where the spoke were etched by means of e-lithography tapering from 200 nm at their touching tips to 10 μm. When displayed on an optical device with given resolution, even a printer or PC display, the spokes appear to merge into a central disk, which gives the overall resolution of the imaging setup. Our Siemens stars were fabricated using a Si_3N_4 membrane with a thickness of 100 nm and a Cr absorber layer of 20 nm.

3. Results and discussion

3.1. Design optimization

Computational pre-studies were done to define (i) the optimum design for the given optical elements available, and (ii) a sensitivity study to define how much impact on performance was to be expected by any potential experimental mismatch upon assembling the setup. Fig. 4 summarizes major findings. An "E"-shaped mask was imaged consistently with the experimental constraints given above, and the calculated images are shown.

The condenser adjustment shows (Fig. 4a–b) a sensitive impact on the illumination even for 1% axial offsetting from optimum. In fact, the condenser produces an image of the source that ideally should fall at the sample plane. A closer positioning of the condenser to the sample with respect to the optimum position can enlarge the field of view with concomitant deterioration of the illumination. It should be also noted that given the horizontal tilt between the condenser and the objective, to allow transport of the light beyond the pair, a slight

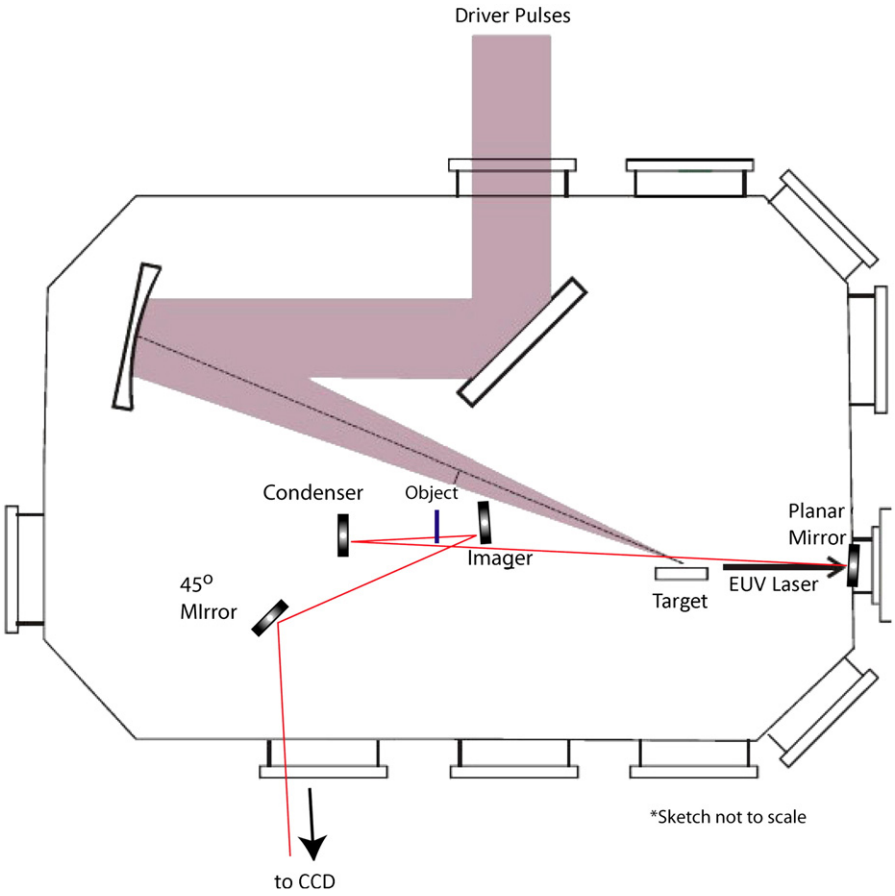

Fig.2. Optical setup of the multilayer imaging illuminated by the table-top EUV laser.

astigmatism is observed. This can be exploited to maximize the photon flux within the width of the detector, i.e. 13.6 mm. The mirror was adjusted for best sample illumination, i.e. 615 mm from the first planar mirror, and optimum range is within 1%.

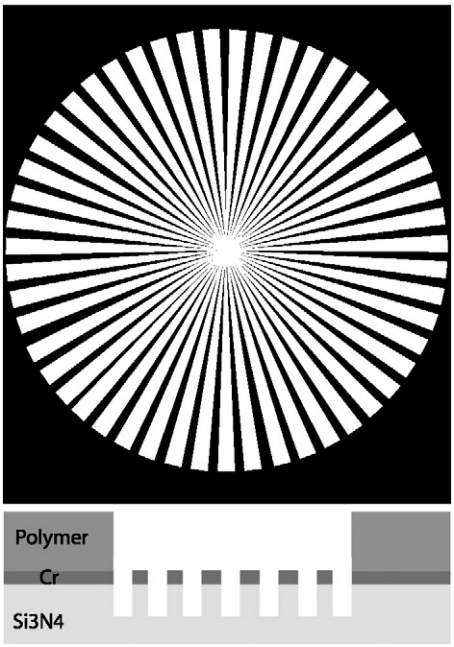

Fig.3. Indicative schematic of the Siemens star sample used. Spokes tapering between 10 and 0.2 μm.

The objective adjustment (Fig. 4c–d) has also an influence on the illumination, since it controls the projection of the source. For maximized illumination the mirror-pair distance was matched to the source distance to obtain an infinite-corrected projection. Concomitantly, the objective performs the 12× imaging of the sample. The mirror was thus adjusted for best CCD illumination, i.e. the condenser-to-objective distance was 266 mm. Mirror tilt was also investigated (not shown in Fig. 4). The observed effects were (i) an obvious horizontal stretching of the image, and (ii) the formation of a vertical illumination stripe. The maximum recommended tilt angle, also to avoid drastic loss of multilayer reflectivity, was 5°. We have finally chosen to operate at 3° tilt angle.

Last issue that was subject of raytracing investigations was the influence of photon counts (Fig. 4e–h) on the imaging quality. In fact, we wanted to validate that our four-element design would not cause a drastic loss of illumination. Further, we have investigated whether with a repeated number of EUV shots we could compensate for illumination loss. In the raytracing computation the conversion was approx. 13:1 rays-to-photons. As Fig. 4 summarizes one notes that for more than 10^4 collected photons across the full field-of-view, the image contrast is good. Our table-top laser source is expected to provide above 10^{10} photons/shot. Considering that a spontaneous emission laser plasma source offers factor of 10^6 less brightness/pulse, due to the emission over 4π sr, we conclude that good contrast at single-shot operation can be obtained with a EUV laser source only. Thus one single shot was found to be sufficient to produce high-contrast images. We investigated the benefit of accumulating additional shots to enhance signal-to-noise ratio (Fig. 4i–l). The results indicate that the optimization of the beam collimation is much more significant than accumulation of sequential shots. Moreover, considering that in the present system the repetition rate is extremely low (1 shot every 12 min), accumulation is also very

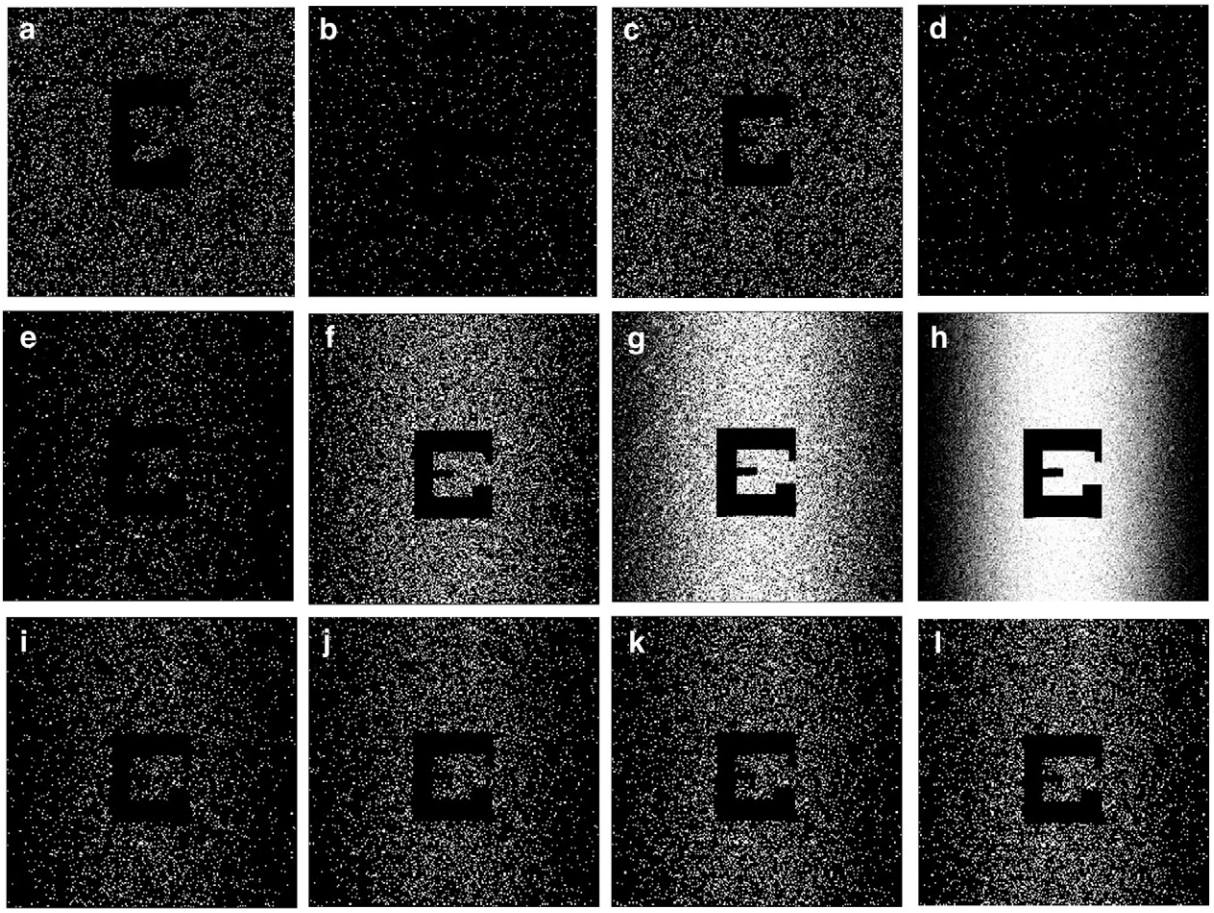

Fig.4. Calculated images by means of raytracing, with the EUV microscope specifications given in the experimental section. Legend: a) condenser 2 mm back from reference position, b) condenser 2 mm ahead of reference position, c) objective 2 mm back from reference position, d) objective 2 mm ahead of reference position, e) 10^5 rays exposure (rays to photons ratio is 13:1), f) 10^6 rays exposure, g) 10^7 rays exposure, h) 10^8 rays exposure, i) 2 shots of frame "e", j) 3 shots of frame "e", k) 4 shots of frame "e", l) 5 shots of frame "e".

time-consuming and can be practically restricted to just a few shots as shown in Fig. 4i–l.

3.2. Experiments

The sample was located between the spherical mirror pair in the object plane, with its position adjusted using a XYZ translation stage. Images were taken of a Siemens star to assess the performance in terms of resolution, contrast and astigmatism. The bright-to-dark contrast was measured for three traces at the spoke edge (Fig. 5). Contrast γ is defined as $(I_{max}-I_{min})/(I_{max}+I_{min})$ and its mean value was found to be $\gamma = 61 \pm 6\%$, with practically a vertical edge, and limited by radiation halo around the transmissive spoke. We can argue that the recalculated results, corrected for stray radiation, are showing enhanced contrast. In fact, it is evident that the zone beyond the bright spoke is not fully blocking the probe radiation. A 4:1 intensity contrast was measured, whereas the Siemens star should provide bright and completely dark zones juxtaposed. To explain the observed 4:1 values it is likely that in-band stray light from the spontaneous component has reached the exposure chamber. If this is the case, any additive flare term "*c*" that superimposes to the *max* and *min* intensity values, does not change the contrast *max–min*, yet the computed γ is degraded as follows:

$$\frac{dy}{dc} = \left[\frac{(I_{max}+c)-(I_{min}+c)}{(I_{max}+c)+(I_{min}+c)}\right]' = -\frac{2(I_{max}-I_{min})}{(I_{max}-I_{min}+2c)^2}. \quad (1)$$

This relation indicates that in our case, based on measured background values, the theoretical contrast is as high as 74%, in agreement with the obtained modulation transfer function (see below).

Fig. 6 shows three contrast profiles of the exposed Siemens star along circular traces obtained at R = 20, 60, and 100 pixels from the Siemens star center. The illumination profile is influenced by the

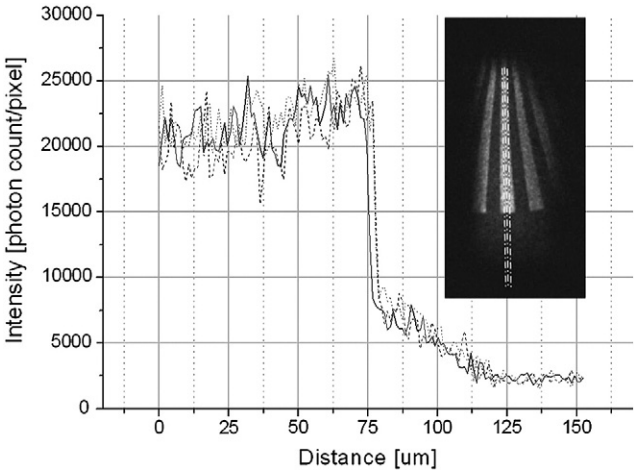

Fig.5. Illumination profiles at the Siemens star's bottom edge, showing the bright-to-dark contrast.

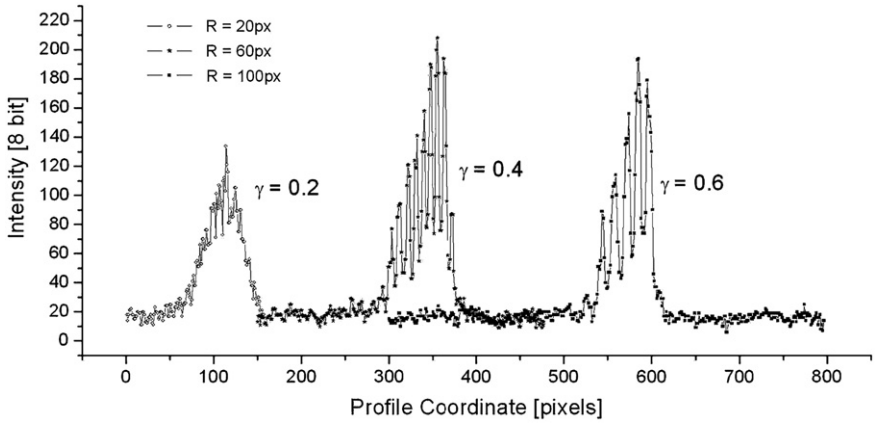

Fig.6. Contrast profiles at three different radial distances (radii in pixels) from the Siemens star center. The corresponding contrast values (γ) are given.

minimal astigmatism introduced by horizontal tilting of the condenser and objective, as discussed above in the raytracing section. The number of photons was estimated from the counts and the CCD quantum efficiency which is 45% at 103.7 eV (12-nm Sn laser line). The average areal illumination was characterized by a relative 1σ deviation (RSD) of 9% over the entire illuminated field. Knowing the collected image counts and considering the reflectivity of the Mo/Y mirror array, and the transmissivity of Si_3N_4 membrane (sample) and Zr foil (filter) as given in the experimental section, we could determine the source photons generated to be as high as 10^{11} photons that correspond to 1.8 μJ, in agreement with previous energy calibration experiments. The improvement of contrast at lower spatial frequency, i.e. at the Siemens star periphery, is evident. This can be quantified by means of the modulation transfer function (MTF).

We have computed the MTF for the unprocessed images, and also for images where an additional image processing was applied. The latter aimed at improving the background correction. The background correction was done considering a rolling ball radius of 10, 30, or 50 pixels around every pixel of the image. The obtained images after post-processing are shown in Fig. 7. In Fig. 8, the MTF is given for the four cases, where the case with 10 pixels rolling ball radius is not shown for clarity since it was identical to the unprocessed image. One notes that the image processing procedure did improve the resolution limit (MTF = 0.5) of a factor 2.5, from 300 to 800 lp/mm. The present resolution is limited by the available optics NA. Further improvement is underway since we are developing a system based on the use of large NA EUV optics, with either Schwarzschild multilayer or Fresnel zone plate.

The importance of using a coherent source for high quality inspection/imaging is experimentally demonstrated in Fig. 9. The image was a single coherent (LHS)–incoherent (RHS) snapshot (no stitching). One notes the difference between the region illuminated

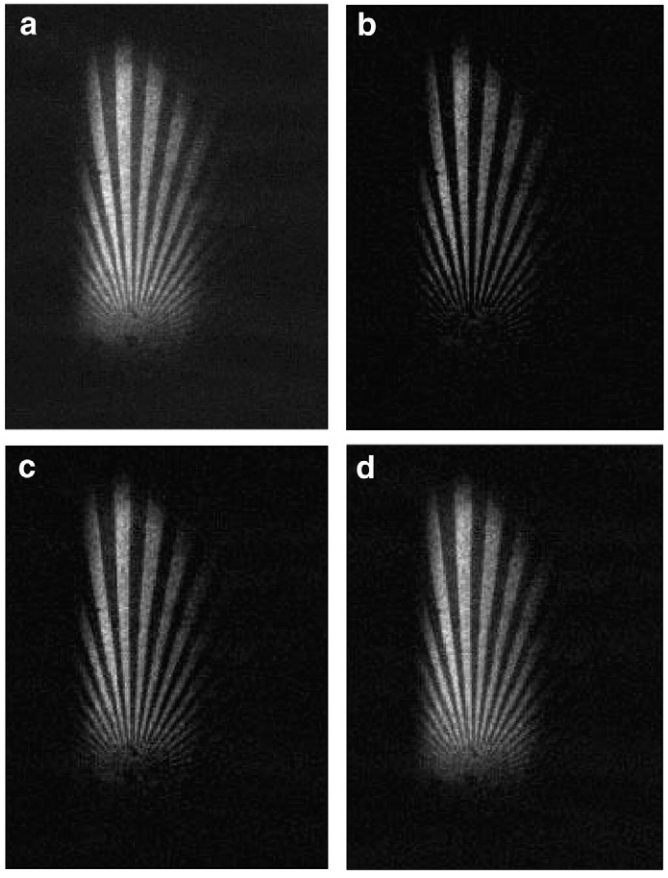

Fig.7. Contrast improvement applying different background correction criteria, versus the unprocessed EUV image. Legend: a) unprocessed image, and background correction from b) 10 pixel rolling ball radius c) 30 pixel rolling ball radius and d) 50 pixel rolling ball radius.

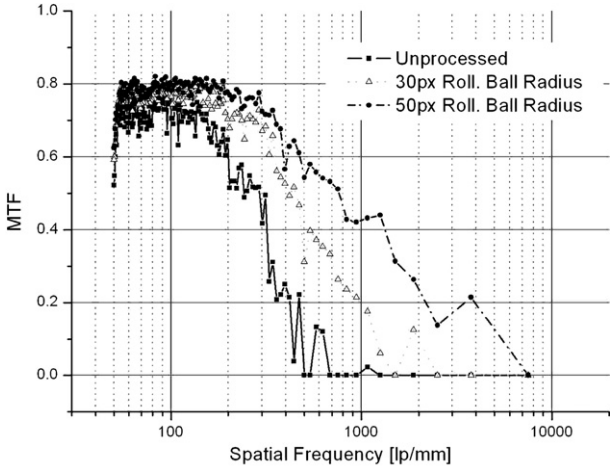

Fig.8. Modulation transfer function as a function of Siemens star spatial frequency expressed as line pairs per mm (lp/mm). Different curves refer to cases discussed in Fig. 7, where background subtraction with 10 pixel rolling ball radius did not show substantial difference with unprocessed curve.

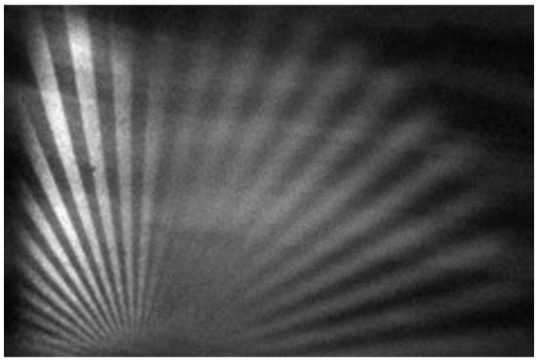

Fig. 9. Comparison of coherent (LHS) versus incoherent (RHS) EUV illumination for imaging.

by the coherent beam (LHS) and the region illuminated by the incoherent light (RHS). The latter provides poorer sharpness, contrast and illumination, which can be assessed observing the outer edges of the Siemens star's spokes (see discussion above). Thus despite an increased source energy (4.4 μJ) the lack of collimation in the extended RHS region of Fig. 9 has a detrimental effect on the overall image quality.

4. Future work

The two-mirror design discussed here, i.e. *condenser* and *imager*, is made-up of two juxtaposed concave spherical multilayer reflectors. Considering that the EUV light must be transported within and beyond the mirror pair gap, i.e. where the Siemens star was mounted, a certain tilt angle (here 3°) has to be tolerated. The tilt induces astigmatism and coma aberrations in proportion to the cosine of the tilt angle. In order to address these drawbacks, we plan to extend our measurement campaign using a concave–convex mirror pair (i.e. a Schwarzschild objective) [10]. Schwarzschild objectives have been demonstrated [11,12] to provide an aberration-free imaging with exactly two mirrors, and also of being capable of high resolution as required in EUV lithography. Fig. 10 shows the dramatic improvement in imaging quality and resolution in the vertical and horizontal dimensions when Schwarzschild optics (Fig. 10b) is compared to the tilted two-concave-mirror design (Fig. 10a), thanks to the collinear light transport. In spite of the dramatic improvement in resolution (values given in Fig. 10), it remains however that the here investigated system acts as condenser/imager pair with two reflections only, whereas Schwarzschild optics uses already two reflections for just imaging, and potentially another two, if one needs to have a condenser. Thus, considering a single multilayer reflectivity of 45% at 12 nm, the two concave-mirror-design studied

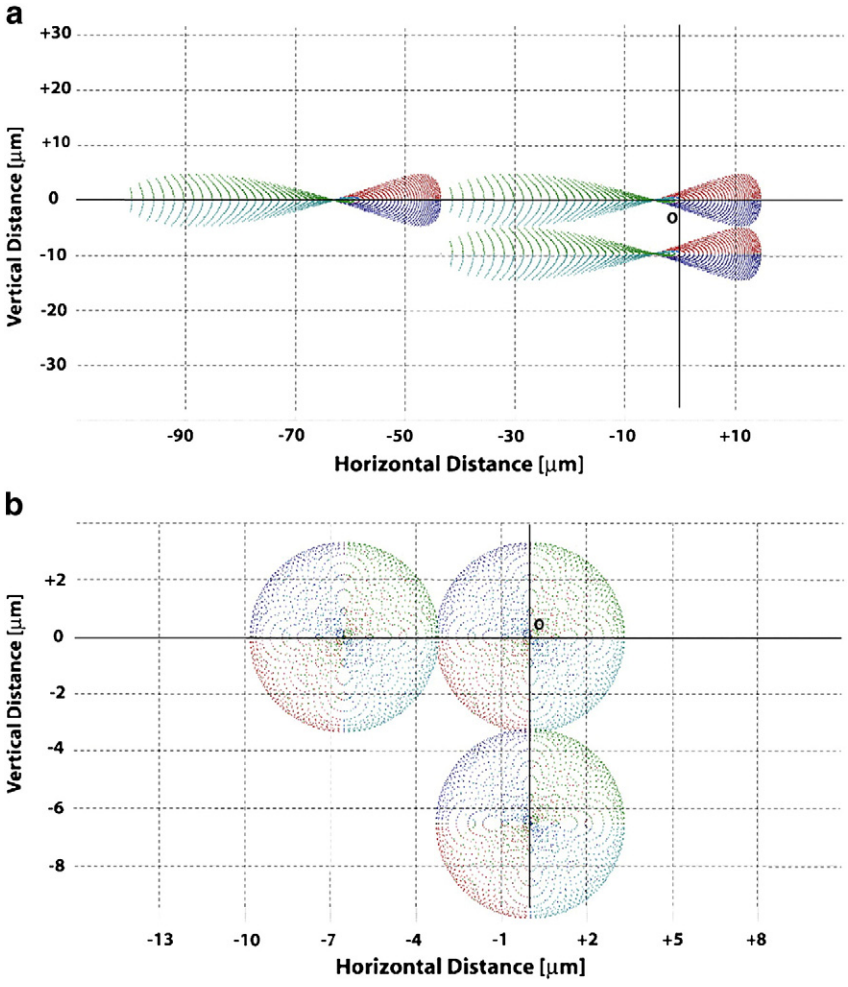

Fig. 10. Imaging spot diagrams obtained by raytracing of (a) 3° tilted concave mirror with a radius of curvature of 241.3 mm; (b) Schwarzschild objective with 50-fold magnification . The four quadrants have different colors as follows: green (NW), red (NE), blue (SE), cyan (SW). The imaging is shown for three points to visualize the vertical and horizontal resolution limit (spots edge-contact). For the case in (a) the resolution is 3 μm horizontal and 0.5 μm vertical. For the case in (b) the resolution is 0.13 μm horizontal and 0.13 μm vertical.

here allows an overall light throughput of 20% whereas the dual Schwarzschild design would allow as low as 4.1% overall throughput.

5. Conclusions

The semiconductor industry is striving for moving on towards next generation lithography in due time to sustain growth trends. This is not only a matter of high volume manufacturing sources, but implies access to lab-scale bright EUV sources for mask defect inspection. The production yield is indeed a function of lithographic throughput and yield. With many workers having demonstrated the feasibility of lithography in the EUV, the remaining challenge is that of scaling-down the tools. Plasma sources can be integrated as high repetition rate sources for fabrication, and under ASE lasing scheme, also as high brightness sources for inspection. A compact footprint imaging source is here demonstrated, whose spatial resolution is limited by the optics NA, not by the source characteristics. Henceforth, full scalability to higher magnification is possible, without any severe loss of illumination, if a EUV laser is used. The ability to direct 10^{11} photons to a field-of-view of several tens of microns with a single shot, permits to obtain high signal-to-noise ratio images rapidly, without need for time-consuming signal accumulation. Moreover, single-shot operation with a pulse duration of a few ps ensures that mechanical vibrations of the systems are not of concern.

Acknowledgements

The University of Berne, the Swiss National Science Foundation, and the Holcim Stiftung have funded parts of this work. The COST MP0601 Action “Short wavelength Laboratory Sources” has supported exchanges and discussions with European partner laboratories. V. Bakshi, (EUV Litho), J. Gobrecht and Ch. David (Paul Scherrer Institute) are acknowledged for stimulating discussions. The authors are grateful to Ch. Imesch and B. Locher for support.

References

[1] V. Bakshi (Ed.), EUV Sources for Lithography, SPIE Press Monograph vol PM 149, 2006.
[2] G. O'Sullivan, A. Cummings, C.Z. Dong, P. Dunne, P. Hayden, O. Morris, E. Sokell, F. O'Reilly, M.G. Su, J. White, ‘Emission and absorption in laser produced plasmas: processes and applications’, J. Phys. Conf. Series 163 (012003) (2009) 1–8.
[3] A. Sasaki, A. Sunahara, K. Nishihara, T. Nishikawa, K. Fujima, T. Kagawa, K. Koike, H. Tanuma, Atomic modelling of the plasma EUV sources, High Energy Density Phys. 3 (2007) 250–255.
[4] H. Fiedorowicz, A. Bartnik, R. Jarocki, J. Kostecki, J. Mikolajczyk, R. Rakowski, M. Szczurek, Laser plasma light source based on a gas puff target for EUV metrology applications, Microprocess. and Nanotechnol. 7954075 (2003) 314.
[5] M. Richardson, D. Torres, Ch. DePriest, F. Jin, G. Shimkaveg, Mass-limited, debris-free laser-plasma EUV source, Opt. Commun. 145 (1998) 109–112.
[6] R. Rakowski, J. Mikołajczyk, A. Bartnik, H. Fiedorowicz, F. de Gaufridy de Dortan, R. Jarocki, J. Kostecki, M. Szczurek and P. Wachulak, *Laser-produced plasma EUV source based on tin-rich, thin-layer targets*, Appl. Phys. B: Lasers & Optics 102, 559–567.
[7] S. Suckewer, P. Jaegle, X-ray Laser: past, present, and future, Laser Phys. Lett. 6 (2009) 411–436.
[8] J.C. Chanteloup, E. Salmon, C. Sauteret, A. Migus, P. Zeitoun, A. Klisnick, A. Carillon, S. Hubert, D. Ros, P. Nickles, M. Kalachnikov, Pulse-front control of 15 TW pulses with a tilted compressor, and application to the subpicosecond travelling-wave pumping of soft-x-ray laser, J. Opt. Soc. Am. B 1 (7/1) (2000) 151.
[9] J. Nilsen, S. Bajt, H.N. Chapman, F. Staub, J.E. Balmer, Mo:Y multilayer mirror technology utilized to image the near-field output of a Ni-like Sn laser at 11.9 nm, Opt. Lett. 28 (2003) 2249.
[10] K. Scharzschild, Abh. Wiss. Goett. Math. Phys. K1 NF4, 1 (1905).
[11] 2.I.G. Artioukov, K.M. Krymski, Opt. Eng. 39 (2000) 2163.
[12] 3.S. Bollanti, et al., Appl. Phys. B85 603 (2006).